Flash-Induced Relaxation Changes of the EPR Signals from the Manganese Cluster and Y_D Reveal a Light-Adaptation Process of Photosystem II†

Sindra Peterson,‡,§ Karin A. Åhrling,|| Joakim E. P. Högblom,‡ and Stenbjörn Styring*,‡

Department of Biochemistry, Center for Chemistry and Chemical Engineering, Lund University, PO Box 124, S-22100 Lund, Sweden, and Photobioenergetics, Research School of Biological Sciences and Department of Chemistry, Faculties of Science, Australian National University, Canberra ACT 0200, Australia

Received September 13, 2002; Revised Manuscript Received January 8, 2003

ABSTRACT: By exposing photosystem II (PSII) samples to an incrementing number of excitation flashes at room temperature, followed by freezing, we could compare the Mn-derived multiline EPR signal from the S_2 oxidation state as prepared by 1, 5, 10, and 25 flashes of light. While the S_2 multiline signals exhibited by these samples differed very little in spectral shape, a significant increase of the relaxation rate of the signal was detected in the multiflash samples as compared to the S_2-state produced by a single oxidation. A similar relaxation rate increase was observed for the EPR signal from $Y_D^{\bullet}$. The temperature dependence of the multiline spin−lattice relaxation rate is similar after 1 and 5 flashes. These data are discussed together with previously reported phenomena in terms of a light-adaptation process of PSII, which commences on the third flash after dark-adaptation and is completed after 10 flashes. At room temperature, the fast-relaxing, light-adapted state falls back to the slow-relaxing, dark-adapted state with $t_{1/2} = 80$ s. We speculate that light-adaptation involves changes necessary for efficient continuous water splitting. This would parallel activation processes found in many other large redox enzymes, such as Cytochrome *c* oxidase and Ni−Fe hydrogenase. Several mechanisms of light-adaptation are discussed, and we find that the data may be accounted for by a change of the PSII protein matrix or by the light-induced appearance of a paramagnetic center on the PSII donor side. At this time, no EPR signal has been detected that correlates with the increase of the relaxation rates, and the nature of such a new paramagnet remains unclear. However, the relaxation enhancement data could be used, in conjunction with the known Mn−Y_D distance, to estimate the position of such an unknown relaxer. If positioned between Y_D and the Mn cluster, it would be located 7−8 Å from the spin center of the S_2 multiline signal.

Photosystem II (PSII)[1] is a membrane-bound enzyme consisting of 25−30 protein subunits, situated in the thylakoid membrane of cyanobacteria and higher plants (*1*, *2*). As a part of the photosynthetic light reactions, it participates in the production of the energy-rich compounds ATP and NADPH. It also performs the energetically demanding task of water oxidation, thereby supplying the atmosphere with molecular oxygen. To this means, light-driven electron transport through the PSII reaction center is performed.

The electron transport chain is initiated when P680, a chlorophyll assembly in the heart of the PSII reaction center, is excited by light energy, by way of the light-harvesting pigments. The short-lived excited state of P680 rapidly donates an electron to a nearby Pheophytin *a* molecule (Pheo). This primary charge separation is stabilized through the oxidation of $Pheo^-$ by a plastoquinone (Q_A) on the stromal side of PSII, which in turn is oxidized by a second plastoquinone (Q_B). After two such reductions, Q_BH_2 leaves the site and is replaced by a new plastoquinone. On the electron donor side of PSII, charge stabilization is achieved when $P680^+$ is rereduced by Y_Z, a redox-active tyrosine residue on the D1 protein. The oxidized $Y_Z^{\bullet}$ is rapidly reduced by the oxygen-evolving complex (OEC), which ultimately extracts electrons from water. In this way, light-induced electron transport is maintained though the PSII reaction center, moving electrons from H_2O on the lumenal side of the membrane to the quinone pool on the stromal side.

The OEC contains four Mn ions, a Ca, and a Cl ion. Extensive X-ray spectroscopy studies of spinach-derived PSII

† Financial support from the Knut and Alice Wallenberg Foundation, the Swedish Natural Science Research Council, DESS, the Swedish National Energy Administration, and the Wenner-Gren Foundations is gratefully acknowledged. K.Å. is supported by an Australian Research Council postdoctoral fellowship.

* Corresponding author. Phone: +4646 2220108. Fax: +4646 2224534. E-mail: stenbjorn.styring@biokem.lu.se.

‡ Lund University.

§ Current address: Research School of Chemistry, Australian National University, Canberra ACT 0200, Australia.

|| Australian National University.

[1] Abbreviations: ATP, adenosine triphosphate; Chl, chlorophyll; Cyt, cytochrome; DMSO, dimethyl sulphoxide; EPR, electron paramagnetic resonance; MES, 2-(*N*-morpholino)ethanesulphonic acid; NADPH, nicotinamide adenine dinucleotide phosphate; NMR PRE, nuclear magnetic resonance proton relaxation enhancement; OEC, oxygen evolving complex; $P_{1/2}$, power of half saturation; P680, primary electron donor of PSII; Pheo, pheophytin; PPBQ, phenyl-*p*-benzoquinone; PSII, photosystem II; RT, room temperature, regulated to 21 ± 1 °C; T_1, spin−lattice relaxation time; T_2, spin−spin relaxation time; Y_D, tyrosine residue D2-Y161; Y_Z, tyrosine residue D1-Y161.

10.1021/bi026848c CCC: $25.00
Published on Web 02/12/2003

have yielded metal-to-metal distances within the OEC (*3*−*5*), which have been utilized to construct various possible structural models of the OEC (see e.g., refs *4* and *6*). The X-ray crystal structure of oxygen-evolving PSII from thermophilic cyanobacteria was presented recently (*7*−*11*), at a resolution of 3.7−3.8 Å. At this resolution, exact structural information on the Mn cluster cannot be derived from the density map. Thus, while the location of the Mn cluster is unambiguously determined by the crystal structure, the molecular scale structure of the OEC is still unclear.

For every four photooxidations of P680, the OEC oxidizes two molecules of water, evolving one molecule of O_2 and four protons in the process. The four-step cycle performed by the OEC to achieve this is called the S-cycle and involves the S_0, S_1, S_2, S_3, and S_4 oxidation states (*12*, *13*). The index signifies the number of electrons that have been removed from the cluster in each state, with the S_0-state the most reduced form of the OEC during water oxidation. Each photooxidation of P680 causes the OEC to progress one step in the cycle. Upon the fourth such oxidation, the OEC is converted from the S_3-state to the S_4-state, O_2 is evolved, and the cluster is rereduced and reset in the S_0-state.

When left in the dark, the OEC equilibrates to the S_1-state, which is the most stable redox configuration. The S_2-, S_3-, and S_0-states are semi-transient and can be trapped by various methods. Particularly, the S_2-state has been studied extensively in PSII samples that have first been dark-adapted, then illuminated continuously at 200 K to form the charge separated state $S_2Q_A^-$ (*14*). The S_2-, S_3-, and S_0-states are all accessible through the flash−freeze method, in which they are trapped by exposing PSII samples to 1, 2, or 3 short, strong flashes of light at room temperature and subsequently freezing them within the lifetime of the S-state in question (*15*, *16*).

Y_D is a conserved tyrosine residue on the D2 protein (*17*−*19*). Although it is redox active, it does not participate directly in the water oxidizing reactions, and its role is not clear. When stored in the dark, PSII centers poised in the S_0-state are converted to the S_1-state through oxidation by $Y_D^{\bullet}$, with a half-time of 50 min at room temperature in PSII membrane fragments (*20*).

Electron paramagnetic resonance (EPR) spectroscopy has proved a powerful method to study the PSII electron transfer chain, particularly the Mn cluster. EPR signals arising from all the semi-transient S-states have now been discovered (reviewed in ref *21*). In the S_2-state, the OEC gives rise to a hyperfine-structured signal at $g = 2$ called the S_2 multiline signal (*22*). In the S_0-state, a broader signal with different hyperfine splitting is visible (*23*, *24*) if a few percent (v/v) methanol has been added to the sample. This amount of methanol affects most of the Mn-derived EPR signals (*25*) (e.g., inducing maximal multiline intensity in samples poised in the S_2-state), but it does not affect enzymatic activity (*25*, *26*). The EPR signals have contributed information on the different S-states in terms of spin states, Mn oxidation states, and exchange interactions within the OEC (*21*). A definite interpretation of these parameters from the EPR signals may soon be possible, with the emergence of a detailed structure of the OEC.

One method of extracting information from EPR signals that has proven very useful is progressive microwave power saturation studies of the spectra. The power of half-saturation ($P_{1/2}$) of a signal is proportional to the spin−lattice relaxation rate, T_1^{-1}, and the spin−spin relaxation rate, T_2^{-1}. Since $T_1 \ll T_2$ for Mn (*27*), spin−lattice relaxation is the dominating contributor to $P_{1/2}$ for the OEC. Furthermore, the EPR signals from the Mn cluster are inhomogeneously broadened, rendering lifetime broadening unimportant. Consequently, T_2 does not contribute significantly to the temperature dependence of the saturation properties of these EPR signals, and $P_{1/2} \propto T_1^{-1}$ (*28*). This has made it possible to investigate spin−lattice relaxation phenomena with the microwave power saturation method, in studies of PSII (*16*, *29*−*34*) as well as other systems (*28*, *35*, *36*). The validity of this approximation is confirmed by the temperature dependence of T_1^{-1} of the S_2 multiline signal, which is very similar when measured by $P_{1/2}$ measurements (*29*, *31*, *34*) and by pulsed-T_1 measurements (*37*, *38*).

The spin−lattice relaxation rate is indicative of interactions between the paramagnetic center and its surroundings and can be analyzed in terms of the accessibility of excited states (if Orbach processes dominate), local connectivity in the protein (if Raman processes dominate), or relaxation enhancement through dipolar interactions with other paramagnets. When such dipolar interactions are present, they can be used to determine distances between paramagnetic centers. This approach has been successful in determining the distance between Y_D and the Mn cluster (*16*, *33*, *39*−*41*), P680 and the Mn cluster (*41*), Y_D and the non-heme Fe (*41*−*43*), Y_Z and the non-heme Fe (*43*), and the Mn cluster and the non-heme Fe (*41*). The recent crystallographic progress has verified these distance estimations (*8*, *11*).

It has been reported that the magnetic properties of the OEC and Y_D are dependent on the extent to which the PSII sample is dark-adapted prior to the experiment (*44*, *45*). As a majority of the spectroscopic studies of the OEC—including EPR, UV−vis, and X-ray spectroscopy—have been performed within the first cycle of oxygen evolution, it is of great relevance to establish whether the conditions of the first cycle are representative of those that prevail during continuous water splitting. In this study, we have taken the combination of EPR spectroscopy and the flash−freeze method further than before, exposing the PSII samples to 1−5, 10, and 25 flashes of light. This enabled us to study the OEC as it passed through more than two full enzymatic cycles of oxygen evolution. Through the use of EPR microwave power saturation, we discovered subtle differences between the first, nearly always studied cycle and the following enzymatic cycle, further removed from dark-adaptation. Our data, analyzed in conjunction with previous reports in the discussion, imply the occurrence of a light-adaptation process of PSII that occurs during the first turnovers of the enzyme.

Such an adaptation is not unprecedented among the large redox enzymes: several enzymes take on one configuration when inactive and a different configuration during continuous enzymatic activity. *Rhus* laccase, for instance, only exhibits maximal activity rates after a full catalytic cycle has been completed (*46*). Isolated Ni−Fe hydrogenase requires two transitions before becoming enzymatically capable: first deoxygenation leads from the unready to the ready form of the enzyme, then a reductive activation takes place (reviewed in ref *47*). Cytochrome *c* Oxidase needs to be completely reduced (four electrons more reduced than the resting state)

and then subjected to a pulse of O_2 before it can oxidize cytochrome *c* at a high rate (*48*).

In our current report, we present data suggesting that the dark-adaptated PSII undergoes a similar process when illuminated. The effect is less drastic than those of the above-mentioned enzymes, as the oxygen-evolving activity of PSII is maximal already at the third flash after dark-adaptation. However, the light-adaptation may well be necessary for continuing efficient water-splitting. What, then, constitutes the light-adaptation process, and how different is the well-characterized dark-adapted form of PSII from the continuously active, light-adapted form? Our observations indicate a need for more spectroscopic analysis to be performed in later cycles of PSII turnover. Caution must be taken not to build all mechanistic discussion on results obtained during the first enzymatic cycle.

MATERIALS AND METHODS

PSII-enriched membrane fragments were prepared from liquid culture grown spinach as described by Pace et al. (*31*) and stored at −80 °C in a buffer containing 0.4 M sucrose, 20 mM MES pH 6.0, 10 mM NaCl, 10 mM $MgCl_2$, and 5 mM $CaCl_2$. Unless otherwise specified, samples for EPR were prepared at room temperature, which throughout this study was regulated to 21 ± 1 °C. The EPR samples were diluted to 4 mg chl/mL, and methanol was added to a final concentration of 5% (v/v). The samples were illuminated with white light for 2 min, then dark-adapted for 15 min. Each sample was then exposed to one laser flash and dark-adapted for 15 more minutes. This preflash protocol renders full oxidation of Y_D and close to 100% of the OEC centers poised in the S_1-state (*15*, *16*). After the preflash treatment, the electron acceptor phenyl-*p*-benzoquinone (PPBQ), dissolved in dimethyl sulfoxide (DMSO), was added to the samples to a final concentration of ∼0.5 mM PPBQ. Each sample was exposed to the appropriate number of laser flashes and frozen within 2 s of the last flash in a dry ice/ethanol bath (198 K), then transferred to $N_2(l)$.

The flashes were delivered at 5 Hz by an Nd:YAG laser (532 nm, 400 mJ) with a pulse length of 7 ns to avoid double hits. Continuous wave EPR was performed on a Bruker E500 spectrometer, fitted with an Oxford Instruments He flow cryostat.

RESULTS

Determining the S-State Specificity of Our Flash−Freeze Samples. A single flash moves the preflashed PSII centers to the S_2-state, two flashes move them to the S_3-state, and three flashes move them to the S_0-state, etc. A miss parameter is associated with the flash protocol; in a good set of samples each flash brings 85−90% of the Mn centers forward in the S-cycle. This results in a gradual dephasing of the PSII centers as the number of flashes is increased.

A full series of samples was prepared, given 1, 2, 3, 4, and 5 flashes, respectively. By measuring the intensity of the S_2 multiline signal in each sample, the size of the S_2-state population was determined as a function of flash number. This yielded an average miss-factor of 13%, which was then used to estimate the S-state composition of each sample. The results are tabulated in Table 1. From these S-state distributions it is clear that in the series of samples given 1−5 flashes, each sample is strongly dominated by the desired S-state. There is also always a certain population of the previous S-state present. In this study, we also prepared a 10-flash sample (37% $S_2^{(3rd)}$ and 10% $S_0^{(2nd)}$; see Table 1) and a 25-flash sample (25% of each S-state). The 10-flash sample gives a relatively weak S_2 multiline signal, but it still dominates the sample. In the 25-flash sample, the S_2 and S_0 signals are of equal strength. They can be analyzed separately by using peaks of minimal spectral overlap to quantitate the signals.

Table 1: S-State Composition of Samples Given 1−5 Flashes of Light at Room Temperature before Immediate Freezing[a]

no. of flashes	S_0 (%)	S_1 (%)	S_2 (%)	S_3 (%)	$S_0^{(2nd)}$ (%)	$S_1^{(2nd)}$ (%)	$S_2^{(2nd)}$ (%)
0	3	97					
1	<1	15	84				
2	<1	2.3	24	73			
3	<1	<1	5.0	31	64		
4	<1	<1	<1	8.5	35	56	
5	<1	<1	<1	1.9	12	38	48

[a] Calculated using a miss-factor of 13% on every flash, no double hits, and 97% S_1 and 3% S_0 in the zero-flash sample. These parameters yield the best fit to multiline oscillations in a particular 1−5-flash sample series. The same parameters yield a composition of a 10-flash sample of 4% $S_3^{(2nd)}$, 10% $S_0^{(3rd)}$, 25% $S_1^{(3rd)}$, 37% $S_2^{(3rd)}$, and 24% $S_3^{(3rd)}$. 2nd and 3rd represent which cycle after dark adaptation. See text.

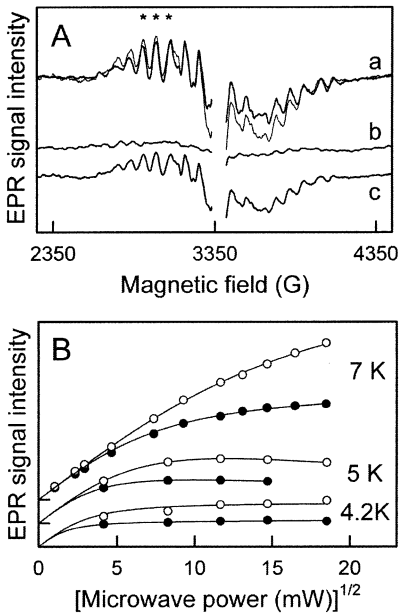

FIGURE 1: (A) The S_2 multiline signal recorded in samples given (a) 1 flash, (b) 4 flashes, and (c) 5 flashes. Thin line: trace c × 1.75. EPR settings: 7 K, microwave power 5.9 mW, microwave frequency 9.47 GHz, modulation amplitude 20 G, and frequency 100 kHz. The asterisks indicate the peaks used for amplitude analysis throughout this paper. (B) Microwave power saturation at different temperatures of the S_2 multiline signal after 1 flash (filled circles) and 5 flashes (open circles). The lines show fits of the data to eq 1.

Line Shape and Microwave Power Saturation of the S_2 Multiline Signal After One and Five Oxidations. The series described above contains two samples poised predominantly in the S_2-state; one that was frozen after a single flash excitation, and one that was frozen after 5 flash excitations. The spectra of these samples are displayed in Figure 1A, along with the 4-flash spectrum. The multiline signal is 1.75 times as strong after 1 flash as after 5 flashes, as discussed

above. The 4-flash spectrum shows almost no S_2 multiline signal; the weak hyperfine structure present is that of the residual S_0 signal. This demonstrates that the 5-flash multiline has indeed appeared after a full turnover of PSII.

The 5-flash multiline signal has been amplified and superimposed on the 1-flash multiline (Figure 1A, thin line). The hyperfine patterns of the two spectra are very similar, although minor variations can be discerned upon careful scrutiny. A separate study of these differences is in progress (K. A. Åhrling, in preparation). The underlying signal is identical in the two spectra.

Figure 1B shows how the intensity of the multiline signal varies with applied microwave power in the two samples, at three different temperatures. Each data set in Figure 1B has been normalized to the same initial slope, thus compensating for the different S_2-state populations in the different samples. Despite this normalization, there is a substantial difference in signal amplitude at high powers between the 1-flash and the 5-flash multiline signals at all three temperatures. Although the multiline signals obtained after 1 and 5 flashes arise from the same formal S-state and appear similar in spectral shape, they have significantly different microwave power saturation behavior.

The data in Figure 1B is well-described by

$$I = I_0\sqrt{P}/\sqrt{(1 + P/P_{1/2})^b} \qquad (1)$$

where I is the measured EPR signal intensity at a certain microwave power P, I_0 is the unsaturated signal intensity, b is the inhomogeneity parameter, and $P_{1/2}$ is the power of half-saturation (*35*). The values of I_0 obtained by fitting eq 1 to the data gave a 5-flash/1-flash multiline intensity ratio at each temperature within 5% of the 48:84 ratio calculated in Table 1. (In Figure 1B, I_0 is set to 1 for clarity for all traces.) At each temperature, the 5-flash $P_{1/2}$ is substantially higher than the 1-flash $P_{1/2}$.

When quantifying the S_2 spectra, we measured the sum of the amplitudes of the three peaks indicated in Figure 1A. These peaks were carefully chosen (*23*) to avoid spectral areas where the S_0 signal is strong in amplitude, thus minimizing the contribution of residual S_0-state centers in the 5-flash sample (12%) to our $P_{1/2}$ determinations. Consequently, the high $P_{1/2}$ of the S_0 signal (*34*) does not contribute significantly to the measured S_2 multiline saturation behavior in the 5-flash sample. In fact, a comparison of these data with our earlier published study (see Figure 4 and ref *34*) reveals that the 5-flash S_2 multiline signal relaxes even faster than the S_0 signal throughout the temperature region displayed in Figure 1B.

In samples bubbled through with Argon for 15 min (and maintained anaerobically) prior to the flash procedure, we found the same difference of relaxation rate between 1- and 5-flash S_2 samples. In summary, while the S_2 multiline signal produced by 5 flashes is spectrally only marginally different from the one produced by a single flash, it displays an inherently higher $P_{1/2}$ than the 1-flash multiline.

Changes at Room Temperature. To investigate the stability of the fast-relaxing form of the S_2 multiline signal obtained after five oxidations of the OEC, we performed the following experiment. A set of 5-flash samples was prepared by the protocol described in Materials and Methods, with one modification: after the excitation flashes were delivered, the samples were not frozen immediately. Instead, they were kept at room temperature in absolute darkness for a monitored period of time, Δt, before freezing. Δt was varied from 2 to 90 s. The value of $P_{1/2}$ (at 5 K) was then recorded for the remaining multiline signal in each sample. The same procedure was used for 1-flash S_2 samples and also for the S_0-state signal in 3-flash samples. The results are displayed in Figure 2.

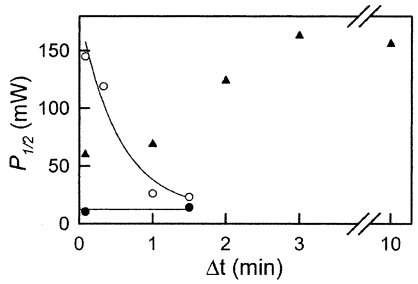

FIGURE 2: Microwave power of half-saturation ($P_{1/2}$) at 5 K as a function of Δt; the period of dark adaptation at room temperature prior to freezing. Closed circles: the S_2 multiline signal after 1 flash. Open circles: the S_2 multiline signal after 5 flashes. Filled triangles: the S_0 signal. The 5-flash data have been fit to an exponential decay with time constant 112 s ($t_{1/2}$ = 80 s) and amplitude 170 mW.

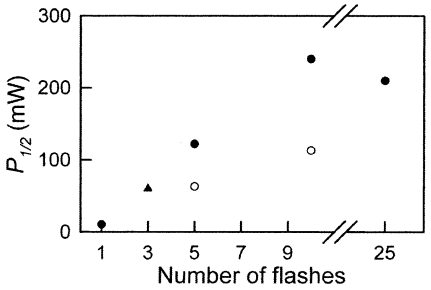

FIGURE 3: $P_{1/2}$ at 5 K as a function of the number of flashes given to the sample before immediately freezing it. Filled circles: the S_2 multiline signal. Open circles: the S_2 multiline signal recorded in the same sample after three weeks of storage at 77 K. Triangle: the S_0 EPR signal.

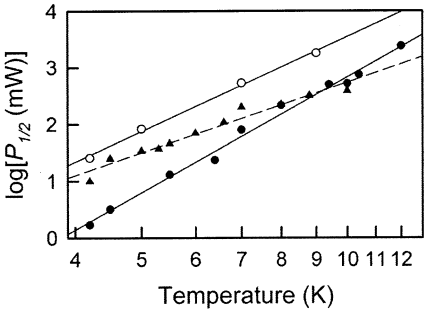

FIGURE 4: $P_{1/2}$ as a function of temperature for the S_2 multiline signal after one flash (filled circles) and five flashes (empty circles) and for the S_0 EPR signal (triangles) on a log−log scale. The fits represent Raman exponents (see text) of 6.8 ± 0.2 for the S_2 multiline signal after one flash, 5.9 ± 0.3 for the S_2 multiline signal after five flashes, and 4.1 ± 0.3 for the S_0 signal.

This experiment was limited in time by the room-temperature decay rate of the S_2- and S_0-states: the decay of the S_2 multiline signal has a half-time of 1.5 min in our samples, and the decay of the S_0 EPR signal has a half-time of 12 min (*23*). As long as the signal is intense enough to be detected at several powers, it is possible to establish a $P_{1/2}$ value for the signal.

Figure 2 shows the change of $P_{1/2}$, measured at 5 K, of the S_0 and S_2 multiline EPR signals during room-temperature dark-adaptation. This does not reflect the decay of the two S-states but reflects gradual changes of relaxation rates of their EPR signals during this time. The S_2 multiline signal in the 1- and 5-flash samples frozen immediately after the flash excitations show the discrepancy in $P_{1/2}$ described above (Figure 1B). During dark-adaptation at room temperature, the 1-flash multiline signal remains at the same low $P_{1/2}$ level. In contrast, the 5-flash multiline shows a decrease of $P_{1/2}$ from the initial fast-relaxing level down to a level similar to that of the 1-flash multiline signal. The fit represents an exponential decay with a half-time of 80 s.

Surprisingly, the microwave power saturation of the S_0 signal also changes during room-temperature dark-adaptation but in a very different, more complex manner. The relaxation rate does not change much during the first minute but then grows dramatically to a maximum level reached after 3 min. The change is of a roughly sigmoidal shape and occurs in the opposite direction to that of the 5-flash multiline signal, producing a faster relaxing S_0 signal after a few minutes of dark-adaptation.

S_2-State After Multiple Turnovers. It is apparent from the data presented above that the Mn cluster undergoes a change during the first turnover after dark-adaptation. This may be part of a process that takes several cycles to complete. To investigate this possibility, we prepared PSII samples given 10 and 25 flashes, respectively. After 10 flashes, the S-state population is rather scrambled, but the S_2-state still dominates with a sample composition of ~37% S_2 centers and only ~10% S_0 centers (see Table 1). Thus, it is possible to study the S_2-state separately from the S_0-state in the 10-flash sample. These S_2 centers are in the third turnover after dark-adaptation. The 25-flash sample is completely scrambled, with 25% of the centers in each S-state. What we can study in such a sample is 25% S_2 and 25% S_0, both several cycles away from dark-adaptation. The values obtained from the S_2 multiline signal in this sample probably contains contributions from the S_0 signal, but the S_2 multiline behavior clearly dominates the strong central peaks used for our amplitude analysis, allowing us to obtain an indication of the S_2 multiline relaxation behavior after multiple turnovers.

The $P_{1/2}$ values obtained for the S_2 multiline signal in the multiple-flash samples at 5 K, displayed in Figure 3 (filled circles), were 240 mW for the 10-flash sample and 210 mW for the 25-flash sample. Such high powers of half-saturation approach the limit of our instrument (360 mW) and are therefore determined with less precision than lower ones. Allowing for some uncertainty because of this, as well as contributions from the slower-relaxing S_0 signal in the 25-flash sample, the obtained 10- and 25-flash values are rather similar. They are both significantly higher than the $P_{1/2}$ of the S_2 multiline in the 5-flash sample, which is 150 mW at the same temperature. These data indicate that the form of the S_2-state present during continuous water splitting is a fast-relaxing form, with $P_{1/2} = 200-250$ mW at 5 K, which is reached after two complete turnovers of a dark-adapted center.

When we remeasured the 5- and 10-flash samples after 3 weeks of storage at 77 K, the $P_{1/2}$ values had receded (Figure 3, open circles). The nonsaturated intensity of these samples, however, had not changed significantly during storage. This implies that the dark-adaptation occurring over minutes at 21 °C (Figure 2) also occurs at 77 K but at a time scale of weeks.

Temperature Dependence of the 5-Flash Multiline Power Saturation. In Figure 4, $P_{1/2}$ of the multiline signal after 1 and 5 flashes, detected in samples that were frozen immediately after flash illumination, is displayed as a function of temperature on a log−log scale. The temperature dependence of $P_{1/2}$ of the S_0 EPR signal is also indicated for comparison. We repeated the measurements on three different 5-flash samples, and all samples gave very similar results to those displayed in Figure 4. The 5-flash data points show clear linearity, with a slope similar to the 1-flash data. This shows that although the 5-flash multiline relaxes faster than the 1-flash multiline signal, the temperature dependence of the relaxation rate is similar in the two samples.

In previous reports (*34*, *49*), we reviewed the accumulated body of published data from differently prepared S_2 and S_0 samples in terms of both Curie plots and relaxation studies. We found that the bulk of the data is most consistent with both the S_0 and S_2 multiline signals relaxing via a Raman mechanism. Given this, we find it reasonable to analyze the present 5-flash S_2 data in terms of the Raman relaxation mechanism as well. The characteristic temperature dependence of the Raman relaxation mechanism is

$$1/T_1 \propto T^n \qquad (2)$$

where $1/T_1$ is the spin−lattice relaxation rate, T is the temperature, and n is the Raman exponent. For an inhomogeneously broadened signal such as the S_2 multiline, the temperature dependence of $P_{1/2}$ is proportional to that of $1/T_1$ (see introductory section), and the Raman exponent n can be derived from the slope of a $\log(P_{1/2})$ versus $\log(T)$ plot such as Figure 4. The exponent obtained from the 1-flash multiline data is $n = 6.8 \pm 0.2$ (*34*), and from the 5-flash data we obtain $n = 5.9 \pm 0.3$. These values are quite similar, in contrast to the S_0 signal that has a Raman exponent of $n = 4.1 \pm 0.3$ (*34*).

The 5-flash data can also be fitted to an Orbach mechanism (not shown), rendering a gap between the ground state and the first excited state of 22 cm^{-1}, as compared to 30 cm^{-1} for a similar fit of the 1-flash data (*34*). However, our data present no evidence of a change of the intrinsic S_2 relaxation mechanism in going from 1 to 5 flashes, making the Raman mechanism the more likely of the two.

$Y_D^\bullet$ Microwave Power Saturation After 1 and 5 Flashes. In our PSII samples, nearly 100% of the Y_D population is oxidized in the preflash protocol (see Materials and Methods) to avoid reactions between the Mn cluster and Y_D, which may reduce the S-state synchrony of the PSII centers in our samples. $Y_D^\bullet$ gives rise to a characteristic EPR signal (Figure 5, inset), the relaxation of which is highly sensitive to nearby paramagnetic centers.

In Figure 5, the 7 K microwave power saturation curves of $Y_D^\bullet$ in a 1- and a 5-flash S_2-state sample are displayed, along with the zero-flash $Y_D^\bullet$ saturation curve for comparison. The inset shows a typical nonsaturated $Y_D^\bullet$ spectrum. The spectral shape is that of pure $Y_D^\bullet$, indicating that there is no other radical formation in the sample. (The half-time of the decay of $Y_Z^\bullet$, which could interfere with our

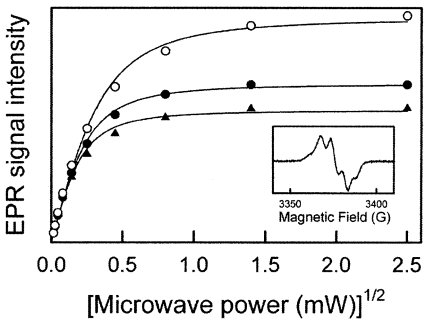

FIGURE 5: Microwave power saturation of the EPR signal from $Y_D^\bullet$ at 7 K in samples given zero flashes (triangles), 1 flash (filled circles), and 5 flashes (open circles). Inset: the unsaturated spectrum of $Y_D^\bullet$. The signal intensity was obtained by double integration of the modulated spectrum at each microwave power. The fits represent $P_{1/2}$ values of 61 μW for the zero-flash data, 88 μW for the 1-flash data, and 177 μW for the 5-flash data. EPR settings: microwave frequency 9.47 GHz, modulation amplitude 2.0 G, and frequency 3.13 kHz.

interpretation of the $Y_D^\bullet$ data, is at most 1 ms (*50*) and has thus relaxed back when we freeze our samples.)

$Y_D^\bullet$ relaxes faster in the S_2 samples than in the S_1 sample, as expected. For the two S_2 samples, $Y_D^\bullet$ shows the same tendency as the Mn signals, with a more efficient relaxation after 5 flashes than after 1 flash. The fits in Figure 5 represent $P_{1/2}$ values of 88 μW for $Y_D^\bullet$ in the 1-flash sample and 177 μW for $Y_D^\bullet$ in the 5-flash sample. The corresponding value of the zero-flash S_1 sample is 61 μW.

DISCUSSION

Phenomena reminiscent of the Mn-derived relaxation changes described here have been reported earlier from EPR relaxation studies of the Mn cluster and $Y_D^\bullet$ and NMR proton relaxation enhancement (NMR PRE). In the following, we describe briefly the various reports and try to rationalize them in terms of a single light-induced mechanism.

Relaxation Changes in the S_1-State. Brudvig and co-workers (*45*) discovered that the extent to which a PSII sample was dark-adapted after a period of continuous illumination affected the properties of the Mn cluster, such that the S_1-state obtained after a short period of dark-adaptation (6 min at 0 °C) was different from that obtained from a long-term dark-adapted sample (4 h at 0 °C). The two forms of the S_1-state were called active and resting forms, respectively. In samples with the OEC in the resting S_1-state, $Y_D^\bullet$ relaxation was as slow as in Mn-depleted samples. With the OEC in the active S_1-state, $Y_D^\bullet$ relaxation was faster (*44*). It was also found that active centers performed slow oxygen reduction in the dark, while resting centers did not (*45*). The transformation of the S_1-state in the dark from the active to the resting form had a half-time of 30 min at room temperature, as measured by the rate of O_2 consumption (*45*), and 3.5 h at 0 °C, as measured by the relaxation rate of $Y_D^\bullet$ (*44*).

Styring and Rutherford monitored $Y_D^\bullet$ power saturation as a function of S-state in samples prepared by the flash−freeze technique described in Materials and Methods (*16*). They noted that even after correcting the data for residual S_0 and S_2 populations, $Y_D^\bullet$ relaxed significantly faster in a 4-flash S_1 center than in a zero-flash S_1 center. This phenomenon was seen again with pulsed T_1 measurements (*39*). Van Vliet and Rutherford (*51*) found that exposing a thoroughly dark-adapted sample to 1 or 2 flashes of light followed by 10 min of dark-adaptation left the sample in the resting S_1-state, implying that at least 3 flashes are required to change the status of the sample from resting to active (i.e., one full turnover is required for the change to occur).

Relaxation Changes in the S_2-State. The resting and active forms of the S_1-state presented by Brudvig and co-workers differed most notably in the form of the S_2 multiline signal that resulted from low-temperature illumination of the differently prepared S_1 samples (*45*). The multiline signal arising from the resting S_1-state was similar to the one usually reported and was most effectively induced by 200 K illumination. Illumination of the active S_1-state resulted in two different multiline signals, with significantly different hyperfine structure and which gave maximal yield at 160 and 170 K illumination, respectively. The S_2 multiline spectra we obtain by exposing our samples to 1 and 5 flashes at room temperature both resemble the resting state multiline signal of Brudvig and co-workers. This implies that the unusual multiline signals associated with the active state only appear after low-temperature illumination. The mechanism that causes an enhanced relaxation rate in samples prepared by flashes at physiological temperatures may also result in a different response to low-temperature illumination, such as that reported by Brudvig and co-workers.

We report that the transformation of the S_2 multiline signal from the light-adapted to the dark-adapted state has a half-time of 80 s at room temperature (Figure 2). This is significantly faster than the transformation of the active to the resting S_1-state described above (*45*). The difference in rates of inactivation/dark-adaptation between the two studies indicates that PSII poised in the S_2-state converts to the dark-adapted state more efficiently than PSII poised in the S_1-state.

Relaxation Changes in the S_0-State. Styring and Rutherford (*16*) followed a procedure analogous to that of Figure 2: they produced 3-flash (S_0-state) samples and waited different periods of time before freezing them. After freezing, they measured $P_{1/2}$ of $Y_D^\bullet$. They found that the saturation behavior of $Y_D^\bullet$ changed with time in the S_0-state: the initially high value of $P_{1/2}$ receded to a lower value with a half-time of 30 s. While some of this reduction can be ascribed to the decay of the S_2 and S_3 centers present in the 3-flash sample, this only accounts for approximately half of the observed change (see ref *16*). In a later study (*39*), it was shown that the high $P_{1/2}$ first observed from $Y_D^\bullet$ in the S_0-state was due to a temperature resonance phenomenon, indicative of a very strong relaxation enhancer, much stronger than the OEC poised in the S_2-state. But the S_0-state decays with a half-time of 12 min (*23*), and the observed effect had a half-time of 30 s, indicating that the OEC poised in the S_0-state was not the sole cause of the relaxation enhancement on $Y_D^\bullet$ after 3 flashes. Srinivasan and Sharp made a similar discovery when measuring NMR proton relaxation enhancement (PRE) in PSII as a function of S-state (*52*, *53*). After 1 and 2 flash excitations, the proton relaxation rate was enhanced by the increased oxidation state of the Mn. The observed enhancement decayed on the time scale of S_2- and S_3-state decay to the S_1-state. However, the relaxation enhancement induced

Table 2: Summary of the Literature Data Discussed in the Text, Interpreted in Terms of One Dark-Adapted and One Light-Adapted Form of the Mn Cluster throughout the S-Cycle[a]

S-state	dark-adapted	light-adapted	light → dark	source
	4 h dark-adapted:	**6 min dark-adapted:**		
	$Y_D^\bullet$ T_1^{-1} low	$Y_D^\bullet$ T_1^{-1} high	$t_{1/2}$ = 3.5 h at 273 K	*44*
	no O_2 consumption	O_2 consumption	$t_{1/2}$ = 30 min at RT	*45*
S_1	**0 flashes:**	**4 flashes:**		
	$Y_D^\bullet$ $P_{1/2}$ low	$Y_D^\bullet$ $P_{1/2}$ high		*16*
	$Y_D^\bullet$ T_1^{-1} low	$Y_D^\bullet$ T_1^{-1} high		*39*
	$Y_D^\bullet$ $P_{1/2}$ low	$Y_D^\bullet$ $P_{1/2}$ high		*51*
	4 h dark-adapted:	**6 min dark-adapted:**		
	200 K ill ⟹	160−170 K ⟹		
S_2	ordinary S_2 multiline	alternative multilines		*45*
	1 flash:	**5 flashes:**		
	S_2 multiline $P_{1/2}$ low	S_2 multiline $P_{1/2}$ high	$t_{1/2}$ = 80 s at RT	this paper
	3 flashes, after Δt at RT:	**3 flashes, immediately:**		
	$Y_D^\bullet$ $P_{1/2}$ low	$Y_D^\bullet$ $P_{1/2}$ high	$t_{1/2}$ = 30 s at RT	*16*
	NMR PRE low	NMR PRE high	$t_{1/2}$ = 50 s at RT	*52, 53*
S_0	S_0 multiline (fast comp.)	S_0 multiline (fast comp.)		
	$P_{1/2}$ low	$P_{1/2}$ high	$t_{1/2} \approx$ 1 min at RT	this paper
	S_0 multiline (slow comp.)	S_0 multiline (slow comp.)		
	$P_{1/2}$ high	$P_{1/2}$ low	$t_{1/2} \approx$ 2 min at RT	this paper

[a] The present S_0 data has been interpreted in terms of a fast and a slow component. See text.

by 3 flash excitations decayed with a half-time of 50 s, much faster than the S_0-state decay (*23*).

The results described above show, like our present data, a change at room temperature of PSII poised in the S_0-state that is not related to the decay of the S_0 signal intensity. However, the change detected through $Y_D^\bullet$ saturation and proton relaxation is a decay of relaxation rate taking place over a period of 30−50 s. Our results on the other hand, which were measured directly on the Mn-derived S_0 EPR signal, show an increase of relaxation rate over 3 min (Figure 2). A rationalization of these apparently contradicting results may be found in the peculiar shape of the S_0 $P_{1/2}$ increase in Figure 2. It is plausible that the tendency reported here is the sum of two processes: an increase of $P_{1/2}$ occurring over several minutes, accompanied by a decrease occurring over less than 1 min, which also affects $Y_D^\bullet$ and proton NMR relaxation. The sum of these processes would account for the initially unchanging level of $P_{1/2}$ in Figure 2, with the faster process diminishing the effect of the slower process during the first minute. (This hypothesis was originally proposed to us by R. J. Pace.)

In this scenario, one component of the detected $P_{1/2}$ of the S_0 signal shows similar behavior to $P_{1/2}$ of the 5-flash S_2 multiline signal, which decays in 80 s. The additional process affecting $P_{1/2}$ of the S_0 signal, causing the slow increase displayed in Figure 2, is to our knowledge unparalleled in the other S-states.

Light-Adaptation of the OEC. Table 2 summarizes the different findings from the literature and this report. Taken together, it seems that the S_0-, S_1-, and S_2-states of the OEC all come in two different forms, as judged by the relaxation properties of the Mn cluster, $Y_D^\bullet$, and nearby protons. For each S-state, a fast-relaxing form is related to PSII under illumination—light-adapted PSII—and a slow-relaxing form to PSII in the dark—dark-adapted PSII. When left in the dark, the fast-relaxing, light-adapted form transforms into the slow-relaxing, dark-adapted form, at rates that depend on temperature and in which S-state PSII is poised. (The additional, slower process taking place in the S_0-state is not included in this hypothesis.)

These data imply that light-adaptation is a single mechanism of change for all the S-states, which sets in after the second photooxidation of the OEC (*51*) and is completed during the first two turnovers after dark-adaptation (Figure 3). This change may be a necessary preparation for efficient continuous water splitting.

Possible Mechanisms of Light-Adaptation. What constitutes the light-adaptation process? One option, which was proposed by Beck et al. (*45*) to account for the differing multiline signals they were detecting, is a light-induced change of the exchange couplings within the Mn cluster. This may affect the intrinsic relaxation rate of the Mn-derived signals. However, as we detect only minor spectral changes of the multiline signal (Figure 1), this cannot account for the dramatically increased relaxation rate. Even minor modification of the exchange couplings between any of the Mn would cause spectral changes to the multiline signal (*54*, *55*).

A second possibility is that a change has occurred in the protein lattice in which the Mn cluster resides, facilitating the release of excess energy into the surroundings and thereby increasing the power of half-saturation. A light-induced change of the protein surroundings of the OEC as a cause of the relaxation changes would be consistent with the unchanging spectral features of the multiline signal. We cannot exclude this explanation with absolute certainty, but we note that the data in Figure 4 argue against it. A change in the protein network surrounding the paramagnet is expected to result in a different Raman exponent, as this is sensitive to local connectivity (see ref *34* and references therein). The current observation, that the 1- and 5-flash multiline signals relax with very similar temperature dependence of $P_{1/2}$, rather suggests a separate relaxation process with relatively weak temperature dependence being added to the Raman relaxation process.

A third possibility that would account for the light-adaptation data is the appearance of a relaxation enhancer in PSII. This would involve either the formation of a new paramagnetic center in PSII or the conversion of an already existing paramagnet into a form that has a stronger effect

on the relaxation of other species. This is an option that agrees well with our data, and in the following we will explore it in greater detail, beginning by surveying the candidates for such a relaxer.

Possible Relaxation Enhancers in PSII. Although the relaxation behavior of the Mn cluster and $Y_D^{\bullet}$ are in accordance with the presence of a third paramagnetic center nearby, we have not been able to detect any new EPR signal from this relaxer. We conclude that the putative relaxer is not an $S = 1/2$ center, as this would be immediately apparent in our spectra. An integer spin system is a more plausible candidate, although it would have to be broadened to an unusual extent to completely escape detection. The strong effect the relaxer has on the two $S = 1/2$ paramagnets—the S_2-state Mn cluster and $Y_D^{\bullet}$—indicates that it is a faster relaxer than both of them. This, too, speaks for a spin state higher than $S = 1/2$. This restriction excludes amino acid or pigment radicals as well as semi-quinone forms of plastoquinone or PPBQ as sources of the enhancement. Other known redox centers in PSII that may exercise strong relaxation enhancement are the acceptor-side non-heme Fe, cyt b_{559}, and possibly molecular oxygen.

In flash samples, the non-heme Fe oscillates between the two oxidation states with a period of two: $Fe^{II}Q_A$ is present in samples given 0, 2, and 4 flashes, while $Fe^{III}Q_A$ is present in 1-, 3-, and 5-flash samples (*56*, *57*). We can therefore exclude the non-heme Fe as a contributor to the substantial relaxation enhancement detected for the 5-flash multiline signal as compared to the 1-flash signal. Changes of the redox state of cyt b_{559} are easily detected in the multiline spectrum, as a peak at $g = 3$. We detect no oxidation of cyt b_{559} in going from 1 to 5 flashes and conclude that this center is not responsible for the relaxation enhancement observed. Molecular oxygen is a strong paramagnet that is released by the Mn cluster upon the third flash excitation, which has previously been proposed to account for the light-induced relaxation changes in PSII (*51*). Oxygen release kinetics occur on the time scale of milliseconds, and there is no evidence that O_2 rebinds to the site as the oxygen spin probe relaxation remains unchanged (*58*). As the $P_{1/2}$ decay reported in Figure 2 has a half-time of 80 s, this alternative is excluded. Our anaerobically prepared control samples further corroborate this.

Having excluded the known paramagnetic centers of PSII, a remaining possibility is a hitherto unknown even-spin system, exercising strong relaxation enhancement on the Mn cluster but with an EPR signal broad enough to escape detection in perpendicular mode. Two spin-coupled radicals or a radical spin-coupled to a metal may be options. If the multiline signal arises from only part of the Mn cluster (as proposed in ref *59*), the remaining Mn ions may be involved.

Location of the Relaxation Enhancer. If the light-adaptation phenomenon involves the appearance of a relaxation enhancer, the discussion above indicates that this enhancer is a hitherto unknown paramagnetic center in PSII. This center displays no strong EPR signals but affects the EPR signals from $Y_D^{\bullet}$ and the Mn cluster through relaxation enhancement. With the distance between the Mn cluster and $Y_D^{\bullet}$ known, the measured relaxation enhancement of the S_2 multiline signal and of the $Y_D^{\bullet}$ signal can be utilized to estimate the location of a relaxation enhancer affecting them both.

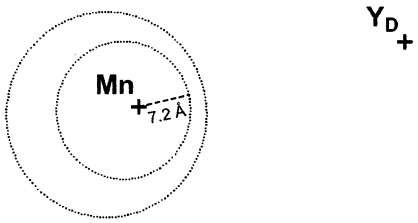

FIGURE 6: Schematic representation of the donor side paramagnets, as viewed along the membrane plane. The crosses represent the spins on $Y_D^{\bullet}$ and the S_2 Mn cluster, 30.8 Å apart as deduced from the crystal structure (*8*). The dotted circles are 2-D representations of the inner and outer spheres that limit the possible locations of the unknown paramagnet, as calculated from its relaxation enhancement on the Mn cluster and $Y_D^{\bullet}$ (see Discussion).

We have made use of the fact that the dipolar interaction between two paramagnets is strongly distance dependent to extract an estimate of the ratio of the Y_D-to-relaxer distance and the Mn-to-relaxer distance from our data (see Appendix). The obtained ratio is $r_{YD}/r_{ML} = 3.66 \pm 0.64$. We can now utilize the known distance between the Mn cluster and Y_D (30.8 Å, as deduced from ref *8*) in conjunction with this ratio to place limits on the possible location of the relaxer. The result of this triangulation is a sphere surrounding the Mn cluster, represented in two dimensions in Figure 6. We have only indicated the upper and lower limits of the estimation, to emphasize the approximate nature of this calculation. The minimal distances are obtained if the relaxer is positioned on a straight line between Y_D and Mn; it is then located 7−8 Å from the Mn cluster and 23−24 Å from Y_D. In the maximally distant position, the relaxer lies 9−15 Å from the Mn cluster and 40−46 Å from Y_D. The intermediate possibilities are distributed over a surface surrounding the Mn cluster, as illustrated in Figure 6.

Note that the locations of the Mn and Y_D in Figure 6 represent the spin centers of these paramagnets, which do not necessarily coincide with the center of the X-ray densities. Particularly the Mn cluster is magnetically complex, and little is known about the actual spin distribution that gives rise to the S_2 multiline signal. However, the similarity of the multiline signal after 1 and 5 flashes indicates that no significant changes of spin distribution have occurred during light-adaptation, thus making the two samples comparable in this fashion.

The very strong distance dependence of the dipolar interaction together with the known Mn-to-Y_D distance makes the calculation feasible, despite the associated uncertainties (detailed in the Appendix). Clearly, the limits in Figure 6 allow for many different possible assignments of the enhancer. For instance, it is intriguing that the redox active tyrosine Y_Z, located 7 Å above the Mn density (*8*, *11*), falls within the area of possible positions of the paramagnet. Irrespective of where on the Mn cluster the unpaired spin of the S_2-state resides, and despite the approximative nature of the calculation, one thing is clear: The proposed relaxer is situated in the direct vicinity of the OEC, almost certainly in the D1 protein.

Induction of the Relaxation Enhancer. If a new paramagnet has been formed in PSII, a redox reaction must be involved. In flash samples, 85−90% of the P680 excitations lead to Mn oxidation. The remaining 10−15%, the misses, may conceivably drive another process such as light-adaptation.

However, we perform our measurements on the centers that are in phase, the ones that display a multiline signal after 5 flashes. In these centers, every photoevent in the PSII reaction center has been utilized to drive the oxygen clock, and these centers are the ones in which we detect the relaxation enhancement. We conclude that light-adaptation does not occur through P680 photooxidation.

A more probable candidate for a redox agent driving the light-adaptation process is the reduced quinones that have accepted electrons from the stromal side of PSII. A possible mechanism of light-adaptation would then be a quinone, after being reduced by the first few flashes, delivering electrons to an unknown species on the PSII donor side. Since quinones are two-electron carriers, and we detect no semiquinone signals, this would involve a double reduction. Some support is given to this hypothesis by the finding that the extent of relaxation enhancement induced in $Y_D^\bullet$ is related to the choice of artificial electron acceptor used (*51*). The possible involvement of the acceptor-side quinones in the light-adaptation process is currently under thorough investigation (K. A. Åhrling, in preparation).

Anomalous Data from Dark-Adapted Centers. While EPR spectroscopists often perform their experiments on PSII after a single photoevent—through a flash or 200-K illumination—many optical experiments are commenced on the second flash after dark-adaptation. This is because, when monitoring PSII optically as a function of flash number, the first-flash data point is unpredictable and fits poorly with the rest of the data set. The presently proposed light-adaptation process may be related to this anomalous first-flash behavior: changes occur after dark-adaptation that are not repeated in a cyclic fashion (see e.g., ref *60*).

Any studies undertaken using PSII samples prepared by a single photooxidation (e.g., illumination at 200 K) should be interpreted with the existence of a light-adaptation process in mind. While such studies have yielded a large body of information on the OEC, the conclusions drawn may not all be applicable to the continuously water-oxidizing, light-adapted form of the system.

APPENDIX

The observed spin−lattice relaxation rate for a paramagnet can be separated into two parts: the scalar component $k_{1\mathrm{scalar}}$ that represents the (isotropic) relaxation rate displayed by the center in the absence of any relaxation enhancer and the angle dependent component $k_{1\theta}$ that represents the dipolar interaction between the paramagnet and another paramagnetic center. Brudvig and co-workers (*42*) have explored the analytical expression for $k_{1\theta}$ and found appropriate approximations for how the non-heme Fe affects Y_D in PSII. Applying this formalism to the Mn cluster requires some caution since this is a considerably more complex paramagnetic system. In the present study, we propose that the Mn cluster is the relaxee, influenced by a strong relaxer. We compare the S_2 multiline signal from two different samples, between which there is almost no change of hyperfine structure. This high degree of similarity indicates that albeit complex, the state giving rise to the multiline signal is unchanged between the two samples. Furthermore, we perform our experiments within a temperature regime where only the ground spin state is populated (*33*). Given these circumstances, we see fit to use the formalism of ref *42* to extract some additional information from our data. Below, we follow their reasoning in an application to $Y_D^\bullet$ and the S_2 Mn cluster, both influenced by an unknown, fast relaxer.

To exert substantial relaxation enhancement on the Mn cluster and $Y_D^\bullet$, the unknown relaxation enhancer must be a more efficient relaxer than both of these. We will designate the fast relaxing enhancer f and the slower relaxing species, which is subject to the enhancement (Mn cluster or Y_D), s. We make the assumption that both the spin−lattice (T_1) and the spin−spin (T_2) relaxation times of the fast species are significantly shorter than that of the slow species: T_{1f}, $T_{2f} \ll T_{1s}$, T_{2s}. We also assume that T_{1f}, $T_{2f} \gg 10^{-11}$ s, which is reasonable for radicals or first row transition metals at X-band excitation frequencies (*27*). When a broad EPR signal such as the S_2 multiline signal is subject to relaxation enhancement by a spin center of a different g value, the enhancement of the signal will vary across the spectrum, with a more efficient enhancement occurring in spectral areas closer to the relaxer. The fact that the relaxation enhancement measured for the multiline signal is as strong in the high-field part of the spectrum as in the low-field part of the spectrum (not shown) indicates that the relaxing species has a resonance around $g = 2$, although we do not detect it. This justifies our last assumption: the fast relaxing, unknown species and the slow species (Mn cluster or $Y_D^\bullet$) have similar g values. Given these conditions, $k_{1\theta}$ can be rewritten in terms of a dipolar rate constant $k_{1\mathrm{d}}$:

$$k_{1\theta} = k_{1\mathrm{d}}(1 - 3\cos^2\theta)^2 \tag{3}$$

where $k_{1\mathrm{d}}$ is defined by

$$k_{1\mathrm{d}} = \frac{\gamma_s^2 \mu_f^2}{6r^6 \omega_s^2 (1 - g_f/g_s)^2 T_{2f}} \tag{4}$$

where γ_s is the magnetogyric ratio of the slow spin, μ_f is the magnetic dipole moment of the fast spin, r is the distance between the two paramagnets, ω_s is the Larmor frequency of the observed, slow spin, T_{2f} is the spin−spin relaxation rate of the fast spin, and g_f and g_s are the g values of the fast and slow spins, respectively (*42*).

Our unknown relaxer interacts dipolarly with two slower spins: $Y_D^\bullet$ and the multiline spin. Taking the ratio between the two dipolar relaxation rates, $k_{1\mathrm{d}}^{(\mathrm{ML})}$ and $k_{1\mathrm{d}}^{(Y_D)}$, allows for many of the unknowns of the fast relaxer to be canceled out:

$$\frac{k_{1\mathrm{d}}^{(\mathrm{ML})}}{k_{1\mathrm{d}}^{(Y_D)}} = \frac{r_{Y_D}^{\ 6}}{r_{\mathrm{ML}}^{\ 6}} \frac{(1 - g_f/g_{Y_D})^2}{(1 - g_f/g_{\mathrm{ML}})^2} \tag{5}$$

γ_s has been taken as γ_e for both cases (*42*) and also canceled out. ω_s is the frequency of the observed spin, which at X-band is $2\pi \times 9.1$ GHz. What remains in eq 5 is an expression for the ratio between the distance between the relaxer and $Y_D^\bullet$ (r_{Y_D}) and the distance between the relaxer and the Mn cluster (r_{ML}):

$$\frac{r_{Y_D}}{r_{\mathrm{ML}}} = \sqrt[6]{\frac{k_{1\mathrm{d}}^{(\mathrm{ML})}}{k_{1\mathrm{d}}^{(Y_D)}} F};\ F = \frac{(1 - g_f/g_{\mathrm{ML}})^2}{(1 - g_f/g_{Y_D})^2} \tag{6}$$

Exact evaluation of the factor F requires knowledge of the exact g value of the relaxer. We do not have that information; however, the 6th root dependence diminishes the consequence of F. We know that $g_f \approx 2$, and for such a system the 6th root of $F = 1 \pm 0.2$. Eqs 3−6 are valid as long as g_f is not identical to g_{Y_D} (2.0046) or g_{ML}(1.9822).

$1/T_1$ is the dominant contributor to $P_{1/2}$ (see introductory section). We have measured the increase of $P_{1/2}$ resulting from the appearance of a relaxation enhancer, $\Delta P_{1/2} = P_{1/2}^{(5-\text{flash})} - P_{1/2}^{(1-\text{flash})}$, from both the OEC and $Y_D^\bullet$. This difference represents the induction of a dipolar interaction, k_{1d}. The 6th root of $\Delta P_{1/2}^{(ML)}/\Delta P_{1/2}^{(Y_D)}$ will be insensitive to any variations in $1/T_2$ and can replace $k_{1d}^{(ML)}/k_{1d}^{(Y_D)}$ in eqs 5 and 6.

We obtained $P_{1/2}$ values for the S_2 multiline signal and $Y_D^\bullet$ at 7 K in six separate pairs of 1- and 5-flash samples. While the multiline data represent the pure S_2-state, the 5-flash Y_D data contain contributions from the 4-flash S_1-state and the 3-flash S_0-state (Table 1). While these bring down the $P_{1/2}$ value of Y_D slightly (*25*) as compared to a pure 5-flash S_2-value, the $1/r^6$ distance dependence of the dipolar interaction renders this effect negligible. The average distance ratio obtained from our measurements, using eq 6 with $F = 1$, is

$$\frac{r_{Y_D}}{r_{ML}} \approx \sqrt[6]{\frac{\Delta P_{1/2}^{ML}}{\Delta P_{1/2}^{Y_D}}} = 3.66 \pm 0.64 \qquad (7)$$

The error limit was deduced from the variation of the data sets. It is worth noting that while separate data sets measured on different days, on different samples, or with different spectrometers may differ in terms of the absolute $P_{1/2}$ values obtained, the ratio of eq 7 varies considerably less.

ACKNOWLEDGMENT

The authors are indebted to R.J. Pace for extremely valuable input.

REFERENCES

1. Bricker, T. M., and Ghanotakis, D. F. (1996) in *Oxygenic Photosynthesis: The Light Reactions* (Ort, D. R., and Yocum, C. F., Eds.) pp 113−136, Kluwer Academic Publishers, Dordrecht, The Netherlands.
2. Diner, B. A. (1998) in *Photosynthesis: Molecular Biology of Energy Capture* (McIntosh, L., Ed.) pp 337−360, Academic Press Inc., New York.
3. Yachandra, V. K., DeRose, V. J., Latimer, M. J., Mukerji, I., Sauer, K., and Klein, M. P. (1993) *Science 260*, 675−679.
4. Yachandra, V. K., Sauer, K., and Klein, M. P. (1996) *Chem. Rev. 96*, 2927−2950.
5. Riggs-Gelasco, P. J., Mei, R., Ghanotakis, D. F., Yokum, C. F., and Penner-Hahn, J. E. (1996) *J. Am. Chem. Soc. 118*, 2400−2410.
6. Carell, T. G., Tyryshkin, A. M., and Dismukes, G. C. (2002) *J. Biol. Inorg. Chem. 7*, 2−22.
7. Zouni, A., Jordan, R., Schlodder, E., Fromme, P., and Witt, H. T. (2000) *Biochim. Biophys. Acta 1457*, 103−105.
8. Zouni, A., Witt, H. T., Kern, J., Fromme, P., Krauss, N., Saenger, W., and Orth, P. (2001) *Nature 409*, 739−743.
9. Shen, J.-R., and Kamiya, N. (2000) *Biochemistry 39*, 14739−14744.
10. Kamiya, N., and Shen, J.-R. (2001) in *PS2001: 12th International Congress of Photosynthesis*, pp S5−002, Brisbane, Australia.
11. Kamiya, N., and Shen, J.-R. (2003) *Proc. Natl. Acad. Sci. U.S.A. 100*, 98−103.
12. Kok, B., Forbush, B., and McGloin, M. (1970) *Photochem. Photobiol. 11*, 457−475.
13. Forbush, B., Kok, B., and McGloin, M. (1971) *Photochem. Photobiol. 14*, 307−321.
14. Brudvig, G. W., Casey, J. L., and Sauer, K. (1983) *Biochim. Biophys. Acta 723*, 366−371.
15. Zimmermann, J., and Rutherford, A. W. (1984) *Biochim. Biophys. Acta 767*, 160−167.
16. Styring, S., and Rutherford, A. W. (1988) *Biochemistry 27*, 4915−4923.
17. Barry, B. A., and Babcock, G. T. (1987) *Proc. Natl. Acad. Sci. U.S.A. 84*, 7099−7103.
18. Debus, R. J., Barry, B. A., Babcock, G. T., and McIntosh, L. (1988) *Proc. Natl. Acad. Sci. U.S.A. 85*, 427−430.
19. Vermaas, W. F. J., Rutherford, A. W., and Hansson, Ö. (1988) *Proc. Natl. Acad. Sci. USA 85*, 8477−8481.
20. Styring, S., and Rutherford, A. W. (1987) *Biochemistry 26*, 2401−2405.
21. Åhrling, K. A., and Styring, S. (2000) in *Probing Photosynthesis: Mechanism, Regulation and Adaptation* (Yunus, M., Pathre, U., and Mohanty, P., Eds.) pp 148−163, Taylor and Francis, UK.
22. Dismukes, G. C., and Siderer, Y. (1981) *Proc. Natl. Acad. Sci. U.S.A. 78*, 274−278.
23. Åhrling, K. A., Peterson, S., and Styring, S. (1997) *Biochemistry 36*, 13148−13152.
24. Messinger, J., Robblee, J. H., Yu, W. O., Sauer, K., Yachandra, V. K., and Klein, M. P. (1997) *J. Am. Chem. Soc. 119*, 11349−11350.
25. Deák, Z., Peterson, S., Geijer, P., Åhrling, K. A., and Styring, S. (1999) *Biochim. Biophys. Acta 1412*, 240−249.
26. Bernat, G., Morvaridi, F., Feyziyev, Y., and Styring, S. (2002) *Biochemistry 41*, 5830−5843.
27. Abragam, A., and Bleany, B. (1970) *Electron Paramagnetic Resonance of Transition Ions*, Dover Publications, Inc., New York.
28. Blum, H., Bowyer, J. R., Cusanovich, M. A., Waring, A. J., and Ohnishi, T. (1983) *Biochim. Biophys. Acta 748*, 418−428.
29. Hansson, Ö., Andreasson, L.-E., and Vänngård, T. (1984) in *Advances in Photosynthesis Research* (Sybesma, C., Ed.) p 1.3.307−1.3.310, Martinus Nijoff/Dr. W. Junk, Hague/Boston/Lancaster.
30. de Paula, J. C., and Brudvig, G. W. (1985) *J. Am. Chem. Soc. 107*, 2643−2648.
31. Pace, R. J., Smith, P., Bramley, R., and Stehlik, D. (1991) *Biochim. Biophys. Acta 1058*, 161−170.
32. Koulougliotis, D., Innes, J. B., and Brudvig, G. W. (1994) *Biochemistry 33*, 11814−11822.
33. Koulougliotis, D., Schweitzer, R. H., and Brudvig, G. W. (1997) *Biochemistry 36*, 9735−9746.
34. Peterson, S., Åhrling, K. A., and Styring, S. (1999) *Biochemistry 38*, 15223−15230.
35. Rupp, H., Rao, K. K., Hall, D. O., and Cammack, R. (1978) *Biochim. Biophys. Acta 537*, 255−269.
36. Oliver, M. E., and Hales, B. J. (1993) *Biochemistry 32*, 6058−6064.
37. Lorigan, G. A., and Britt, R. D. (1994) *Biochemistry 33*, 12072−12076.
38. Lorigan, G. A., and Britt, R. D. (2000) *Photosyn. Res. 66*, 189−198.
39. Evelo, R. G., Styring, S., Rutherford, A. W., and Hoff, A. J. (1989) *Biochim. Biophys. Acta 973*, 428−442.
40. Beck, W. F., Innes, J. B., and Brudvig, G. W. (1990) in *Current Research in Photosynthesis* (Baltscheffsky, M., Ed.) pp 817−820, Kluwer Academic Publishers, Dordrecht, The Netherlands.
41. Kodera, Y., Takura, K., and Kawamori, A. (1992) *Biochim. Biophys. Acta 1101*, 23−32.
42. Hirsh, D. J., Beck, W. F., Innes, J. B., and Brudvig, G. W. (1992) *Biochemistry 31*, 532−541.
43. Koulougliotis, D., Tang, X.-S., Diner, B. A., and Brudvig, G. W. (1995) *Biochemistry 34*, 2850−2856.
44. Koulougliotis, D., Hirsh, D. J., and Brudvig, G. W. (1992) *J. Am. Chem. Soc. 114*, 8322−8323.
45. Beck, W. F., de Paula, J. C., and Brudvig, G. W. (1985) *Biochemistry 24*, 3035−3043.
46. Andreasson, L.-E., and Reinhammar, R. (1976) *Biochim. Biophys. Acta 445*, 579−597.
47. Albracht, S. P. J. (1994) *Biochim. Biophys. Acta 1188*, 167−204.
48. Antonini, E., Brunori, M., Colosimo, A., Greenwood, C., and Wilson, M. T. (1977) *Proc. Natl. Acad. Sci. U.S.A. 74*, 3128.

49. Geijer, P., Peterson, S., Åhrling, K. A., Deàk, Z., and Styring, S. (2001) *Biochim. Biophys. Acta 1503*, 83−95.
50. Razeghifard, M. R., and Pace, R. J. (1997) *Biochim. Biophys. Acta 1322*, 141−150.
51. Van Vliet, P., and Rutherford, A. W. Doctoral Thesis, pp 71−94, Agricultural University, Wageningen, The Netherlands, 1996.
52. Srinivasan, A. N., and Sharp, R. R. (1986) *Biochim. Biophys. Acta 850*, 211−217.
53. Srinivasan, A. N., and Sharp, R. R. (1986) *Biochim. Biophys. Acta 851*, 369−376.
54. Belinskii, M. I. (1994) *Chem. Phys. 189*, 451−465.
55. Boussac, A. (1997) *J. Bioinorg. Chem. 2*, 580−585.
56. Petrouleas, V., and Diner, B. A. (1986) *Biochim. Biophys. Acta 849*, 264−275.
57. Zimmermann, J.-L., and Rutherford, A. W. (1986) *Biochim. Biophys. Acta 851*, 416−423.
58. Razeghifard, M. R., and Pace, R. J. (1999) *Biochemistry 38*, 1252−1257.
59. Åhrling, K. A., and Pace, R. J. (1995) *Biophys. J. 68*, 2081−2090.
60. Rappaport, F., Blanchard-Desce, M., and Lavergne, J. (1994) *Biochim. Biophys. Acta 1184*, 178−192.

BI026848C